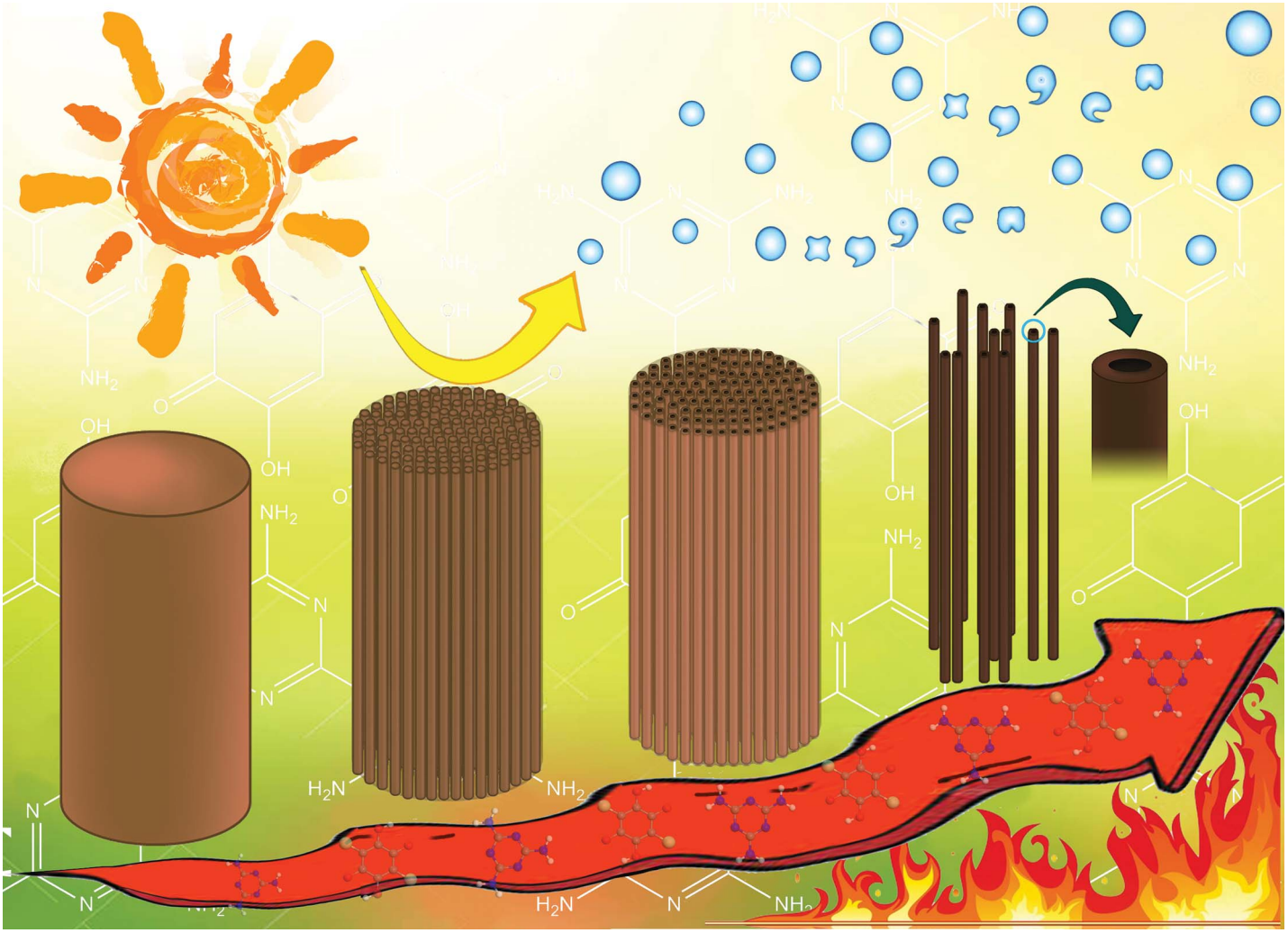

Highlighting research by Lina Li in the group of Innovative Heterogeneous Photocatalysis at Max Planck Institute of Colloids and Interfaces, Germany.

Surface polycondensation as an effective tool to activate organic crystals: from "boxed" semiconductors for water oxidation to 1d carbon nanotubes

A series of materials is prepared by supramolecular preorganization whose morphology could gradually debundle into twisted nanowires, and then hollow carbon tubes with the increase of temperature. During the transition process, the material with just surface polymerization shows high photooxidation potential in organic dye degradation as well as oxygen generation under illumination.

As featured in:

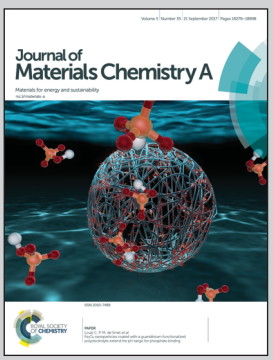

See Lina Li *et al.*, *J. Mater. Chem. A*, 2017, **5**, 18502.

ROYAL SOCIETY OF CHEMISTRY

rsc.li/materials-a

Registered charity number: 207890

Journal of Materials Chemistry A

PAPER

View Article Online
View Journal | View Issue

Cite this: J. Mater. Chem. A, 2017, 5, 18502

Surface polycondensation as an effective tool to activate organic crystals: from "boxed" semiconductors for water oxidation to 1d carbon nanotubes†

Lina Li, *[a] Menny Shalom,[b] Yubao Zhao,[a] Jesús Barrio[b] and Markus Antonietti[a]

Received 10th May 2017
Accepted 10th July 2017

DOI: 10.1039/c7ta04050d

rsc.li/materials-a

A series of materials are prepared by supramolecular preorganization of melamine and chloranilic acid and thermal polycondensation. *Via* the introduction of halogen substitution, the morphology of the supramolecular assembly was successfully altered from 2D plates to 1D nanofibers. The H-bridged crystals are organic semiconductors as such, which however can be massively activated by surface polymerization to create "boxed semiconductors" where the surface layer forms active loci for charge separation and transfer. The resulting polymer coated crystals show high photooxidation potential, as exemplified by Rhodamine B (RhB) degradation, as well as being able to liberate oxygen from water under visible light illumination. The box structure is maintained throughout further thermal condensation, and hollow 1d carbon tubes are obtained at 800 °C.

Introduction

Considering the limits of fossil fuels, it is important to seek new and environmentally friendly substitutes, like hydrogen energy.[1,2] One clean and promising method to produce hydrogen is by light-driven water splitting which uses only water and the abundant solar radiation.[3,4] During the reaction, four electrons and holes are transferred, producing hydrogen and oxygen. The oxygen evolution reaction (OER) is considered to be more challenging due to its sluggish reaction kinetics and the need to transfer 4 electrons and four protons at the same time.[5] Therefore, the efficiency of the OER is currently the limiting factor for the whole photoinduced water splitting cascade, and research on active OER photocatalysts keeps a core position in research on artificial photosynthesis.[6–8]

In recent years, diverse carbon nitride based materials (referred to here as graphitic carbon nitride or g-CN for short), sometimes coupled to earth-abundant co-catalysts, have shown the potential of efficient oxygen production under illumination with visible light.[9–11] For example, the integration of cobalt oxide within graphitic carbon nitride was reported to be an effective method to improve the photocatalytic oxygen evolution process from water.[12] A nanocomposite of carbon nanodot-carbon nitride (C_3N_4) was also reported as a photocatalyst for water splitting, with partly impressive performance.[12,13] Therefore there is good hope that further variations in the electronic structures, local order, and of course nanotexture of these heterogeneous organocatalysts might bring further improvements.

Recently, a new series of g-CN materials have been prepared by our group using supramolecular organization of starting comonomers.[14–16] In a very recent report, we showed the possibility to obtain photoactive organic frameworks by a similar construction principle at relatively low condensation temperatures (~250 °C) which clearly pointed to polymers as the involved species.[17] A series of polycondensates were obtained at different temperatures by starting with a supramolecular assembly with a sheet or better page-like morphology, consisting of melamine and 2,5-dihydroxy 1,4-benzoquinone (DBQ-M).[17] The page-like morphology was formed thanks to the strong multiple hydrogen bonds between the starting monomers. The page-like morphology could be retained up to 800 °C while the C/N ratio and the coupled transformation into a nitrogen doped carbon could be tuned according to the condensation temperature. Even synthesized at comparatively low temperature where the polymerization reaction just sets in, a good photocatalytic activity was found. Experiments of methylene blue photodegradation revealed that both dye reduction and oxidation were enabled under illumination.

It is the purpose of the present article to explore if this reactivity can be improved by employing similar monomers and final one-dimensional structure. Usually, 1D semiconductor materials are highly promising candidates for energy conversion, as charge separation and the consecutive photooxidation/

[a]Department of Colloid Chemistry, Max Planck Institute of Colloids and Interfaces, Potsdam 14476, Germany. E-mail: Lina.Li@mpikg.mpg.de

[b]Chemistry Department, Ben Gurion University of the Negev, Beersheba 009728, Israel

† Electronic supplementary information (ESI) available. See DOI: 10.1039/c7ta04050d

photoreduction can be localized at different ends of the structures.[18] The geometry of the supramolecular assembly is strongly related to the interaction between its components. It was shown that the involvement of halogen atoms can direct the assembly growth toward one dimension.[19,20] Here we present a new series of such materials, ranging from organic crystals and cross-linked polymer semiconductors at lower calcination temperatures to semimetals at higher temperatures, based on supramolecular alignment of melamine and chloranilic acid (CLA) as the starting precursors. The supramolecular assembly of the monomers exhibits a wire-like morphology that can be maintained up to 800 °C, while the C/N ratio again follows the condensation temperature. The photoactive performance of this series is exemplified by photodegradation tests of methylene blue and Rhodamine B. Our results show that a species intermittent between organic crystals and polymers, M-CLA-250, shows an unexpectedly high performance and can efficiently degrade both dyes. Moreover, we found out that M-CLA-250 can act as a photocatalyst for oxygen evolution.

Results and discussion

Synthesis of the M-CLA complex

By mixing CLA and melamine (M) together in water, a new supramolecular B-M-CLA was obtained by overnight crystallization. The yield of this supramolecule may change with the input ratio of CLA and M, and the yield reaches its highest point (99%) when the ratio of CLA and M is about 1 : 2, which we attribute to the preferred intramolecular ratio of CLA and M. The formation of this supramolecular aggregate as a new and distinct entity could be proven by several characterization methods as follows.

Characterization of the M-CLA complex

As shown in Fig. 1a, the B-M-CLA's XRD pattern differs completely from those of the two monomers. In the range of 3–20°, there are almost no overlapping peaks between the complex and monomers. These differences reveal the existence of new larger repeat units within the highly ordered crystal structure. Very relevant for the later condensation and electronic interactions, there are two strong and sharp peaks at 26.5° and 28.0° respectively, corresponding to a graphitic *d*-spacing of 0.335 nm and 0.328 nm. Being tighter than graphite (0.336 nm), these close distances indicate the strong donor–acceptor charge interaction between the layered units. Correspondingly, the UV-vis absorption (Fig. 1b) of the solid B-M-CLA complex differs from those of the monomers, especially in the range of 400–700 nm, where enhanced absorption and a red-shift are observed, representing the appearance of better electron delocalization and polarization within the complexes. The preorganization of the two comonomers *via* H-bridges and the tight mutual packing with extended π–π stacking lead to interlayer electronic transitions and joint electronic systems, very similar to those discussed for and quantified with the nucleobase pairs in DNA resulting in comparably high electronic conductivity.[21,22] Within this joint electronic system, both M and CLA can be regarded as

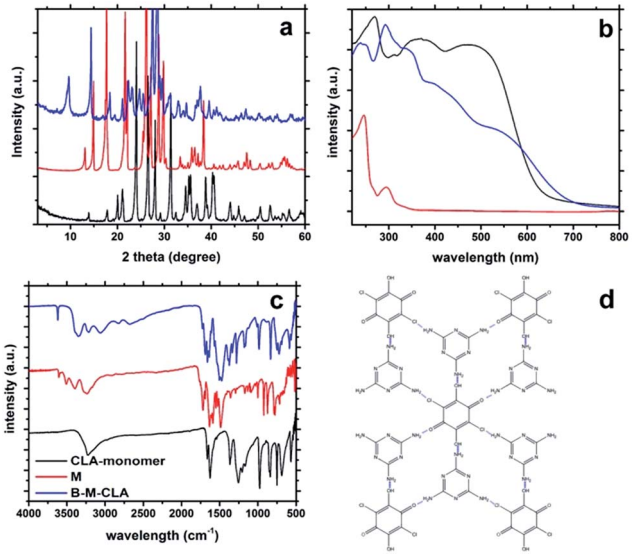

Fig. 1 X-ray diffraction patterns (a); solid UV-vis absorption spectra (b); and Fourier transform infrared spectroscopy spectra (c) of the complex and two raw monomers; schematic complex structure (d). (CLA = chloranilic acid; M = melamine; B-M-CLA = the complex of chloranilic acid and melamine).

very stable tectons, constituting an organic crystalline semiconductor, as further shown below.

Fourier transform infrared spectroscopy (FTIR) measurements also support the complex formation (Fig. 1c). First, some characteristic absorption peaks of CLA vanish, *e.g.* the phenol C–OH stretching vibration at 1260–1180 cm^{-1} and the C=O stretching vibration at 1725–1705 cm^{-1}, which is probably due to the binding to melamine. Similarly the N–H stretching vibration of NH_2 also disappears at *ca.* 3500 cm^{-1}. This phenomenon implies that the newly formed structure strongly interferes with the stretching vibration of the functional groups mentioned above. This indicates that H-bonds are established between amino groups and hydroxyl (or carbonyl) groups, thus constituting the supramolecular assembly. Also, new peaks appear at ~3700 and 3330 cm^{-1}, indicating new vibrations of intramolecular H-bonds. Besides, the C–CI stretching of CLA at around 600 cm^{-1} is obviously weakened in the spectra of the complex, which is consistent with a former report that –Cl can interact weakly with the amino group of melamine.

Also, the formation of the supramolecular complex could also be elucidated by X-ray photoelectron spectroscopy (XPS). As shown in Fig. 2, after the formation of the B-M-CLA complex, the binding energy of N, O and Cl has been adjusted. Compared with chloranilic acid, the Cl 2p peaks of the complex are shifted to 201.7 eV, which just corresponds to the interaction between Cl and NH_2 groups.[23] The O 1s peaks of chloranilic acid are slightly shifted to a lower binding energy area in the complex, which is due to electron transfer during the noncovalent bond formation and the corresponding increase of electron cloud density. The peak at 533.5 eV (C=O bond) varies significantly, which indicates the strong hydrogen bond interaction between C=O and NH_2 groups. For the N 1s peak, its position is shifted

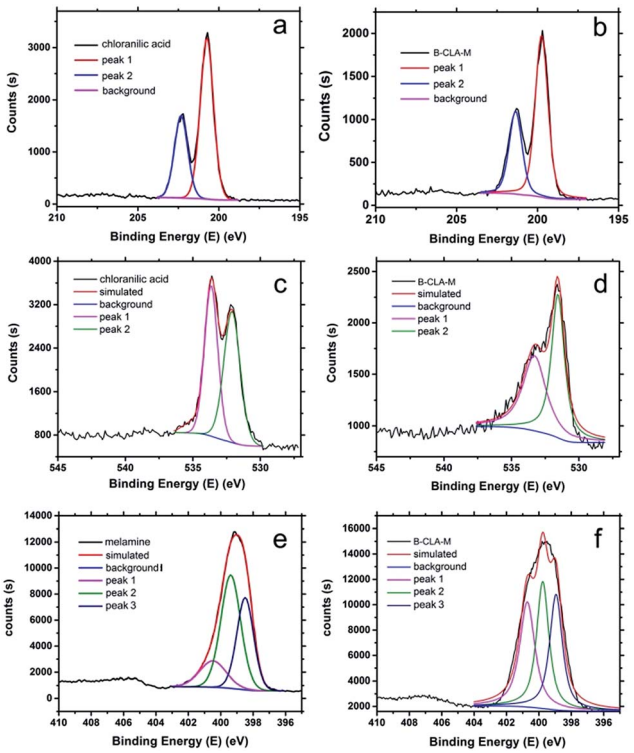

Fig. 2 XPS Cl 2p curves of chloranilic acid (a) and the complex B-CLA-M (b); XPS O 1s curves of chloranilic acid (c) and the complex B-CLA-M (d); XPS N 1s curves of melamine (e) and B-M-CLA (f).

to a higher binding energy area, which indicates that the electron density around N decreases during supramolecular formation, very likely transferring to the surrounding O atoms of chloranilic acid.[24] Together, all this information above indicates the non-covalent bond formation between two monomers. Based on all these data, an illustrative simplification of the supramolecular assembly of CLA and M is shown in Fig. 1d and S1.† In this structure, two melamine molecules interact with one CLA molecule, and they are connected *via* noncovalent forces.

Characterization of B-M-CLA condensed at different temperatures

Applying different condensation temperatures, the B-M-CLA could be condensed into a series of M-CLA-X materials (X = condensation temperature). The exact reaction temperatures and yields are summarized in Table 1. The yields are higher than those found with other melamine-involving materials, owing to the hindrance of the easy sublimation and degradation of melamine, thanks to the strong multiple hydrogen bond networks.

The condensation reaction within the complex could be nicely followed by elemental analysis and thermogravimetry-mass spectrometry (TGA-MS, Fig. 3a). The weight of CLA and the complex remains stable before 100 °C and loses around 8.2% of general weight before 130 °C. This weight loss could likely be referred to as the loss of water bound to the structure, potentially even within the crystalline system. Based on calculations, the mass loss corresponds to two-molecules of water within one supramolecular unit. Then the weight remains unchanged until 200 °C. After that, the aggregate slowly loses another 8.3% until 260 °C, the melting point of the system. This is interesting and most relevant for the further discussion, as such water can be generated only by condensation in premelting structures, *i.e.* surfaces and more disordered grain boundaries. This process is rather well known from other solid state polymerizations, and for instance AH-salts for polyimide synthesis, when carefully heated, polymerize only *via* such molten surface layers.[25] Before 260 °C, the weight ratio of carbon and nitrogen stays at about

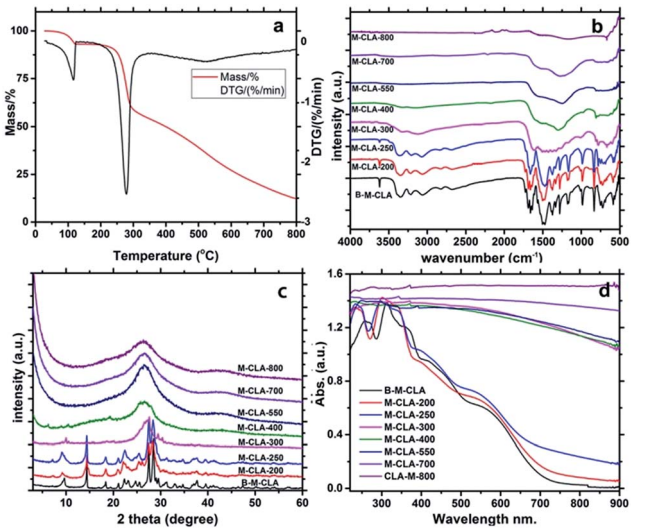

Fig. 3 (a) The TGA mass loss curve of the B-M-CLA complex; FTIR curves (b) and X-ray diffraction patterns (c) and UV-vis absorption spectra (d) of materials obtained at different condensation temperatures.

Table 1 Surface areas, zeta potential and C/N ratio of the resulting materials

	Temperature (°C)	BET ($m^2\ g^{-1}$)	Zeta potential (mV)	C/N mass ratio	Yield
B-M-CLA	25	8.6	−1.56	0.879	0.994
M-CLA-200	25	8.6	−1.56	0.874	0.917
M-CLA-250	250	12.3	−21.6	0.874	0.886
M-CLA-300	300	19.7	27.8	0.845	0.629
M-CLA-550	550	16.8	−28.9	1.159	0.464
M-CLA-800	800	87.8	−16.8	2.680	0.131

0.875, close to the starting situation and fully in agreement with the loss of water only. With the melting, the reaction rather sharply sets in, and the system reduces to 60% remaining mass up to 300 °C. For M-CLA-300, the ratio of C/N decreases, however only slightly to 0.844 together with the great increase of zeta potential, in agreement with the further release of water through completion of polycondensation and release of CO_2 as a side reaction followed by MS (see ESI†). In addition, the total element sum indicates that chlorine is massively lost (probably as HCl) between 250 and 300 °C. This secondary reaction in addition to the condensation by water elimination bridges the ring system to extended aromatic systems and nicely explains the massive narrowing of the band gap. With the further increase of temperature, the weight loss is broad but moderate, and the C/N ratio increases to 1.16 for M-CLA-550 and 2.72 for M-CLA-800. This process is a slow iterative decomposition of the primary material, and the decomposition mainly occurs *via* the release of HCN and N_2.

The continued condensation with temperature can also be followed by FTIR. As shown in Fig. 3b, almost all the infrared characteristic peaks of the complex M-CLA could still be seen in M-CLA-200 and M-CLA-250, proving that the main monomer structure is kept until 250 °C. The coupled mass loss of 12% (see Table 1) is minor and attributed to drying and surface condensation. The main change between M-CLA-250 and M-CLA-300 lies in the range of 650–900 cm^{-1}, which stands for the N–H out of plane deformation vibration. Besides, the intensity of the peak reflecting H-bonding at 3670 cm^{-1} is significantly reduced. The latter elucidates the fact that dehydration between hydroxyl and amino groups is almost completed. In general, all vibration peaks become less distinct, reflecting loss of order and the presence of a polymeric state. Above 300 °C, the IR vibrations of typical functional groups disappear, and the material turns from a polymeric structure into a carbonaceous resin. Only several peaks remain, such as the vibration of the triazine ring at about 800 cm^{-1}, C–N at 1000–1400 cm^{-1} and C=N stretching vibrations at 1500–1600 cm^{-1}. At higher temperatures, the intensity of these peaks decreased along with increasing temperature. Above 550 °C, even the vibration of the triazine ring disappears, along with the usual behavior of triazines to realign into larger aromatic structures at this point. Based on this information, we can simplify that the condensation may take place at about 250 °C, while 550 °C is the starting temperature for ring rearrangement and the formation of the final N-doped carbon.

The condensation process was also analyzed with powder X-ray diffraction (Fig. 3c). Consistent with the FTIR results, the patterns of the materials below 250 °C are very similar to the starting assembly pattern, indicating the maintenance of the main crystal structure. For M-CLA-250, there is a new peak found at around 7.7°, while the peak around 9.3 °C is obviously broadened. These slight changes could result from the starting dehydration within the network. Above 300 °C, the patterns change completely, revealing the melting of the whole crystal structure to form an all-polymeric skeleton. At carbonization and ring rearrangement temperatures, the diffraction peaks further change until only a broad peak at about 27° remains, typical for the interlayer stacking of weakly ordered graphitic carbons. The polymers obviously gradually condense at higher temperatures into N-doped carbon materials.

The solid UV-vis absorption spectra of the synthesized materials (Fig. 3d) follow the electronic changes during the condensation process. At temperatures lower than 250 °C, the spectra are only slightly red-shifted with condensation temperature, indicating weak changes in the bulk structure. Especially the 250 °C sample is still a slightly red shifted version of the primary crystal, *i.e.* the spectrum nicely complies with "a-crystal-in-a-box", where the minor red shift and the tail towards red can be explained by a thin layer of polymer and hetero-junction effects. In accordance with all the structural characterizations, the most significant variation of the light harvesting properties takes place within 250–300 °C. The complex turned into a black polymer resin, presumably a small bandgap semiconductor, while at the highest temperatures the material is totally black, which is typical for an N-doped carbon and its semi-metallic state.

The M-CLA series was further investigated by scanning electron microscopy (SEM) and transmission electron microscopy (TEM). The primary complex of B-M-CLA shows a rod-like morphology (Fig. 4), which is maintained until melting. Interestingly, the structures do melt passing the melting transition, but rather gradually debundle into twisted nanowires at elevated temperatures. This is maybe the most prominent proof that the 250 °C sample indeed undergoes surface and grain boundary polycondensation: melting does not lead to droplets, but rather fills these boxes under preservation of the highly

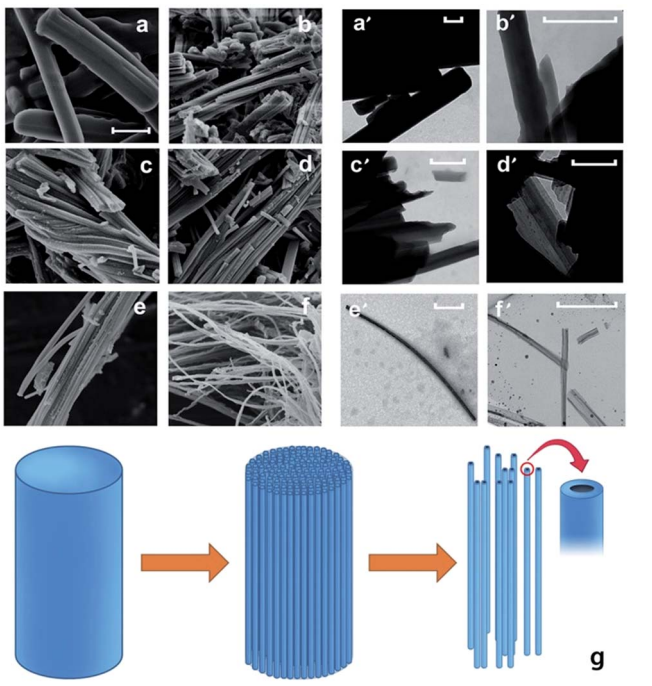

Fig. 4 SEM (left, scale bar equal to 500 nm) and TEM (right, scale bars 1 μm) images of B-M-CLA (a), M-CLA-200 (b), M-CLA-250 (c), M-CLA-300 (d), M-CLA-550 (e), and M-CLA-800 (f); the simplified variation of morphology with temperature (g).

anisometric structures. The surface polycondensation structure could be observed from the high resolution TEM image in Fig. S4,† which shows that the tube-like structure is wrapped with a half transparent cover with around 5 nm thickness. Notably, the nanowires obtained at 800 °C are hollow, *i.e.* are nanotubes, corresponding to the highest mass loss and degree of densification of these structures, however starting from the outside of the first formed polymers.

Compared with the complex of DBQ and M from our previous work, the morphologies of the resulting materials in this work show a fiber-like structure instead of a sheet-like structure. The significant variation in the morphology mainly comes from the introduction of 2 chloride atoms into the CLA monomer that restricted the lateral growth of the primary supramolecular monomer crystals. As an electron withdrawing group, the presence of Cl greatly decreases the electron density of the six-atom ring, which leads to an acidity increase of the hydroxyl group, and the interactions between hydroxyl groups and amino groups are getting stronger. The latter can also explain the higher product yields.

The local structural changes at the bond level during the heating process were also elucidated by X-ray photoelectron spectroscopy (XPS) as shown in Fig. 5. The structural variation could be clearly resolved within the N 1s XPS curves presenting different connection modes with other atoms. The most important N 1s peaks of the complex can be divided into 3 groups, which are at around 400.8 eV (hydrogenated nitrogen), 399.8 eV (charge depleted amine) and 398.8 eV (nitrogen in the triazine ring). The peaks at 400.8 eV reflect the presence of NH_2, which interacts with OH from CLA. At higher temperatures (*e.g.* 250 and 300 °C), this peak disappears, presenting the possible pathway of dehydration within the supramolecular crystal. With further elevation of temperature into the aromatization region, a new peak at 401 eV appears for M-CLA-550, revealing the formation of quaternary nitrogen. Another newly emerging peak at 398.3 eV, indicating nitrogen in C–N, reflects the disintegration of triazine rings and aromatic rearrangements.

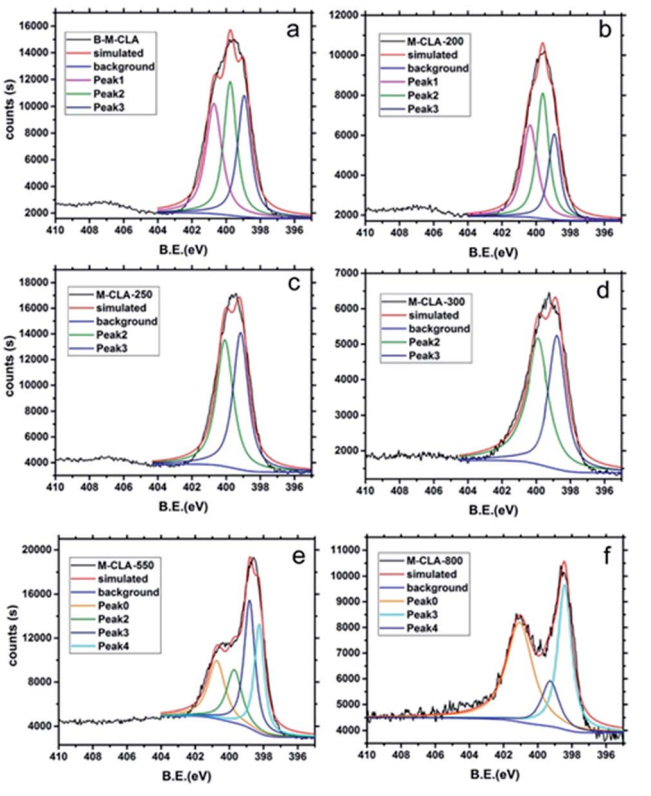

Fig. 5 XPS N 1s curves of B-M-CLA (a), M-CLA-200 (b), M-CLA-250 (c), M-CLA-300 (d), M-CLA-550 (e) and M-CLA-800 (f).

The photoactivity of all the resulting materials was tested by the degradation of Rhodamine B (RhB) under white light illumination (350 nm ~ infrared radiation). For the degradation experiments, about 5 mg of M-CLA materials were added into a 30 mL glass bottle with 20 mL of RhB solution (1 mg L^{-1}). After stirring in the dark for 2 hours, the remaining RhB concentration was tested by UV-vis spectra at the wavelength of 554 (RhB). Although showing different degradation rates, all these materials successfully decomposed both dyes. Based on further experiments in 3 different pure lights, it was found that blue light (445 nm) and green (520 nm) light could degrade RhB while orange (590 nm) light cannot (ESI Fig. S8†).

Most relevant and unexpected, among all the samples, M-CLA-250 shows the best degradation performance. 5 mg of M-CLA-250 could decompose 90% of 20 mL of 1 mg L^{-1} RhB in 4 hours. In order to provide further proof about degradation, colorless phenol was also selected as a degraded matter. As a result, colorless phenol could also be slowly degraded by CLA-250. The pH of the phenol solution decreased from 5.5 to 4 after degradation, indicating that phenol was degraded into oxalic acid and succinic acid. In fact, the photoactivity and light absorption of M-CLA-250 are based on the those of B-M-CLA the primary complex crystal. Obviously, the supramolecular crystal is already a visible light active, H-bridge stabilized, organic semiconductor as such, whose RhB degradation takes double the time of M-CLA-250. But the tiny layer of polymer on top with its different electronic structure of course acts as a heterojunction and improves the effectiveness of charge separation and subsequent charge transfer. This "boxed" organic semiconductor obviously outperforms all other species, as it combines crystalline order and coupled excellent charge transport with the stability of a polymer for stabilization and charge transfer.

In order to confirm the mechanism of the RhB degradation, electron acceptors, such as Ag^+ and oxygen, were introduced into the degradation system (Fig. 6a). As a result, an acceleration of the degradation was observed, indicating that the degradation process mainly occurs through photogenerated holes. Furthermore, the introduction of hole scavengers strongly hindered the dye photodegradation, underpinning our postulation. The relative kinetics of the degradation reaction was calculated, as shown in the ESI.† The formation of peroxide during the degradation process was monitored with peroxide tests, unveiling the existence of OH radicals at a concentration of ~3 μg L^{-1}.

The photogenerated holes can obviously oxidize water, resulting first in the formation of OH radicals that can further recombine to form peroxide, which finally oxidizes RhB

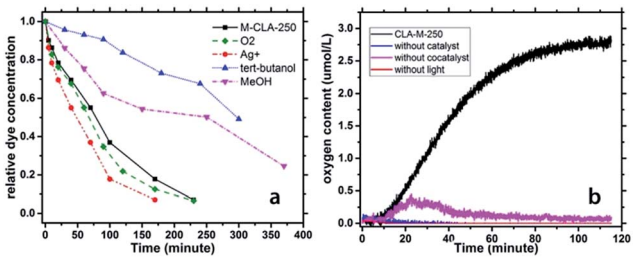

Fig. 6 (a) Photochemical RhB degradation curves with different additives; (b) oxygen production under illumination with M-CLA-250 as a catalyst and control experiments.

molecules into colorless fragments. Moreover, the fact that even peroxide was formed indicated that the valence band (VB) of CLA-250 is significantly more positive than 1.763 eV *vs.* the NHE – the minimum energy that is required to form peroxide. Therefore, the VB of the CLA-250 is sufficient to fully oxide water into molecular oxygen (which is energetically easier than the formation of peroxide, but kinetically hindered as it requires the simultaneous transfer of 4 electrons and four protons). Indeed, we found out that M-CLA-250 without a cocatalyst can generate very low amounts of oxygen. Using cobalt oxide as a cocatalyst can accelerate the 4 electron process. 100 mg of the Co doped M-CLA-250 material was added into the reaction flask together with 200 mg of $AgNO_3$ and 100 mL of water. Then the whole reaction system was flushed with nitrogen for 5 minutes to remove oxygen. The experimental setup was exposed to visible light, while the oxygen content was monitored (Fig. 6b). The concentration of oxygen in water increases with illumination time and reached a maximum amount of 2.8 μmol L^{-1} after 110 minutes. In the first 50 minutes, the oxygen generation showed the highest rate at around 0.05 μmol L^{-1} min^{-1}. After that, the oxygen production process slowed down, probably due to the self-oxidation of the catalyst and the deposition of Ag on the photocatalyst surface that inhibits the water oxidation process.

Conclusions

In this work, we demonstrated that by careful selection of starting monomers and using their supramolecular pre-organization, we can successfully create photoactive systems at relatively low condensation temperatures. Using chlorine substitution to restrict lateral growth, highly ordered fiber-like structures were formed. The optical and catalytic properties as well as the carbon and nitrogen ratio of the materials can be tuned according to the calcination temperature while the fiber-like morphology is preserved up to 800 °C. The material that was prepared at 250 °C undergoes polycondensation only on grain boundaries and its surfaces, but this "boxed" crystalline organic semiconductor shows the highest photocatalytic activity of the whole series toward the degradation of dyes, driven by a very high VB stability and the corresponding strong oxidation capacity. The materials' ability to oxidize is so strong that OH-radicals and finally oxygen can be produced from water under illumination with white light, a process that previously only the more stable g-CN materials can accomplish. We believe that this work can open many opportunities for rational 1D material design as well as for new materials for photooxidation reactions for both organic synthesis and environmental remediation. "Boxed" crystalline organics can therefore be understood as a new paradigm.

Acknowledgements

We thank the members of the research group Nanojunction Design for Uphill Photosynthesis/MPIKG for useful discussions and related technicians of Colloid Chemistry/MPIKG, like Dr Guigang Zhang for discussion on the OER, Rona Pitschke for TEM measurements, Tobias Heil for high resolution TEM measurements and Antje Voelkel for the TGA results.

Notes and references

1 W. Lubitz and W. Tumas, *Chem. Rev.*, 2007, **107**, 3900–3903.
2 M. G. Walter, E. L. Warren, J. R. McKone, S. W. Boettcher, Q. Mi, E. A. Santori and N. S. Lewis, *Chem. Rev.*, 2010, **110**, 6446–6473.
3 S. J. Moniz, S. A. Shevlin, D. J. Martin, Z.-X. Guo and J. Tang, *Energy Environ. Sci.*, 2015, **8**, 731–759.
4 R. Marschall, *Adv. Funct. Mater.*, 2014, **24**, 2421–2440.
5 Y. Cheng and S. P. Jiang, *Prog. Nat. Sci.: Mater. Int.*, 2015, **25**, 545–553.
6 A. Tanaka, K. Hashimoto and H. Kominami, *J. Am. Chem. Soc.*, 2014, **136**, 586–589.
7 Y. Xu, M. Kraft and R. Xu, *Chem. Soc. Rev.*, 2016, 3039–3052.
8 Y.-F. Li and A. Selloni, *ACS Catal.*, 2016, **6**, 4769–4774.
9 H. Wang, L. Zhang, Z. Chen, J. Hu, S. Li, Z. Wang, J. Liu and X. Wang, *Chem. Soc. Rev.*, 2014, **43**, 5234–5244.
10 G. Zhang, S. Zang, L. Lin, Z.-A. Lan, G. Li and X. Wang, *ACS Appl. Mater. Interfaces*, 2016, **8**, 2287–2296.
11 G. Zhang, S. Zang and X. Wang, *ACS Catal.*, 2015, **5**, 941–947.
12 J. Liu, Y. Liu, N. Liu, Y. Han, X. Zhang, H. Huang, Y. Lifshitz, S.-T. Lee, J. Zhong and Z. Kang, *Science*, 2015, **347**, 970–974.
13 G. Gao, Y. Jiao, F. Ma, Y. Jiao, E. Waclawik and A. Du, *Phys. Chem. Chem. Phys.*, 2015, **17**, 31140–31144.
14 J. Xu, S. Cao, T. Brenner, X. Yang, J. Yu, M. Antonietti and M. Shalom, *Adv. Funct. Mater.*, 2015, **25**, 6265–6271.
15 T. Jordan, N. Fechler, J. Xu, T. J. Brenner, M. Antonietti and M. Shalom, *ChemCatChem*, 2015, **7**, 2826–2830.
16 Y. Ishida, L. Chabanne, M. Antonietti and M. Shalom, *Langmuir*, 2014, **30**, 447–451.
17 L. Li, Y. Zhao, M. Antonietti and M. Shalom, *Small*, 2016, **12**, 6090–6097.
18 B. Weng, S. Liu, Z.-R. Tang and Y.-J. Xu, *RSC Adv.*, 2014, **4**, 12685–12700.
19 B. Roy, P. Bairi and A. K. Nandi, *RSC Adv.*, 2014, **4**, 1708–1734.
20 M. Prager, W. Sawka-Dobrowolska, L. Sobczyk, A. Pawlukojć, E. Grech, A. Wischnewski and M. Zamponi, *Chem. Phys.*, 2007, **332**, 1–9.

21 Y. Okahata, T. Kobayashi, K. Tanaka and M. Shimomura, *J. Am. Chem. Soc.*, 1998, **120**, 6165–6166.
22 E. Meggers, M. E. Michel-Beyerle and B. Giese, *J. Am. Chem. Soc.*, 1998, **120**, 12950–12955.
23 Y. Liu, J. Li, X. Cheng, X. Ren and T. Huang, *J. Mater. Chem. B*, 2015, **3**, 1446–1454.
24 C. Ronning, H. Feldermann, R. Merk, H. Hofsäss, P. Reinke and J.-U. Thiele, *Phys. Rev. B: Condens. Matter Mater. Phys.*, 1998, **58**, 2207.
25 M. M. Unterlass, F. Emmerling, M. Antonietti and J. Weber, *Chem. Commun.*, 2014, **50**, 430–432.